A NEW MODEL FOR CONCRETE IN COMPRESSION CONSIDERING THE GROWTH OF THE DAMAGE ZONE

N. V. TUE[1] and N. Đ. TUNG[1*]

[1]*Institute of Structural Concrete, Graz University of Technology, Austria*

ABSTRACT

It is generally accepted that the failure of concrete in compression is characterized by the localization of deformation in so-called the damage zone; therefore a definition of the fracture energy of concrete in compression can be introduced. In contrast to the definition of the fracture energy of concrete in tension, there has been no consistent definition for concrete in compression. The reason is the different failure modes of concrete in compression, which depend strongly on the test specimen size and the boundary condition. In this paper, based on the observation of the crack propagation during the failure a mechanism of the localization is proposed. With the proposed mechanism of the localization, the strain-softening behavior of different points in the damage zone is determined.

Keywords: localization of deformation, compressive fracture energy, damage zone.

1. INTRODUCTION

Evidences of the localization can be found by observing the postpeak displacements of specimens with different lengths (van Mier 1984) or by using photogrammetric technique (Torrenti et al. 1991). Because of the localization the postpeak part of the stress-strain curve of a specimen is not only a material property but is dependent on the specimen or measuring length.

Specimen geometry and boundary condition affect also the strain-softening behavior because they affect the size and shape of the damage zone relative to the overall specimen. The softening branch of specimens becomes steeper with decreasing boundary restraint (Kotsovos 1983). With friction between the loading platens and the specimen a shear band initiating from the corner of specimen was observed. The length of the shear band is usually considered as the length of the damage zone by Mode II of failure (Markeset 1993). In specimens with frictionless boundary conditions only splitting cracks were observed (Vonk 1992; Watanabe et al. 2004). The length of the damage zone, which is measured when the peak stress is reached, by Mode I is smaller than that by the crack pattern observation of Mode II. In specimens loaded by steel brushed both the splitting cracks and a shear band may be formed.

Consider the localization, different formulations for the complete stress-strain curve have been

* Corresponding author: Email: n.tung@tugraz.at

proposed. Bazant (1989), Markeset (1993) modeled the softening curve including the localization as a material property, while van Mier (2009) considered the softening as a specimen-machine interaction behavior. In these models the influences of specimen geometry and boundary condition are not yet clear. Models describing the strain-softening behavior by failure Mode I are still rare, mostly only the fracture energy is examined (Rokugo and Koyanagi 1992; Jansen and Shah 1997).

Based on the observation of the crack propagation during the failure by tests without boundary restraint this paper presents a new mechanism of the localization. From the available experimental data the compressive fracture energy is introduced, where the influences of the specimen geometry and the boundary condition are eliminated. A model for the strain-softening in Mode I is presented.

2. MECHANISM OF THE LOCALIZATION OF DEFORMATION

Investigations on the crack formation and propagation (Dhir and Sangha 1974; Shah and Sankar 1987) shown that at about 70 to 90 % of the peak stress microcracks coalesce to form macrocracks. When the load continues to increase the macrocrack formation becomes instable, by reaching the peak stress the instable crack formation forms a small zone of damage, named the *initial damage zone*. With increasing deformation the loading must reduce to avoid a brittle failure. In the *initial damage zone* displacement must continue to soften, consequently the cracks propagate forward, when the lateral deformation is not or slightly restrained by loading platens. Outside the zone where the localization is taking place during the strain softening, unloading occurs.

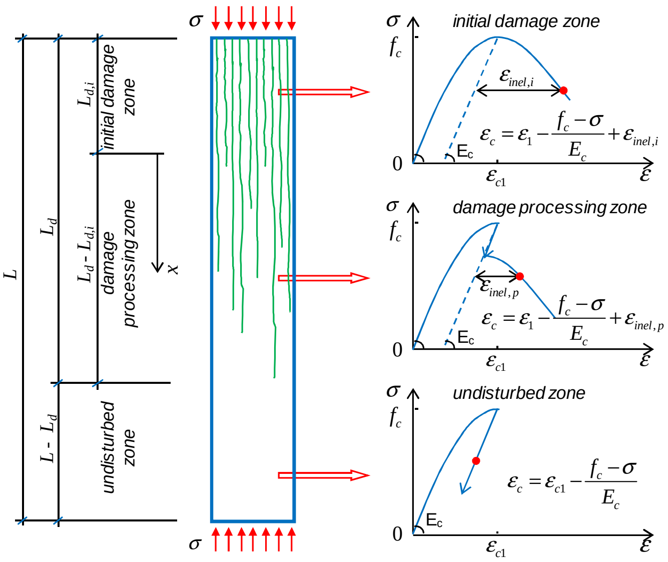

Figure 1: Mechanism of the localization

When the cracks grow to a location, which still lies outside the damage zone by reaching the peak stress, the lateral strain at this location also increases due to the crack opening. Because of the natural relation between the lateral and the longitudinal strains, an increase of the longitudinal strain at this location is expected. Thus the strain behavior of this location changes from unloading to softening. The mechanism of the localization is illustrated in Fig. 1. As long as the specimen stays stable, the crack propagation continues definitely. The closer to the *initial damage zone* the earlier change from the unloading to the softening. The descending branch of the stress-strain curve of this location consists of two portions, i.e. the unloading and the softening parts. This agrees well with the experimental results of Watanabe et al. (2004), whereas local stress-strain curves of different locations were measured by strain gauges embedded at acrylic resin bars. This means that the damage zone does not remain constant during the failure, its length increases. The crack propagation during the failure forms a so-called *damage processing zone*. This phenomenon is also observed by the assessment of the localization using acoustic emission conducted by Puri and Weiss (2006). Through observing the amplitude of acoustic emission on specimen with diameter $D = 100\ mm$, Puri and Weiss found that the length of damage zone by reaching the peak stress is approx. $1{,}2\ D$, while at a strain of $1{,}6\ \varepsilon_{c1}$ the damage zone develops to a length of approx. $2\ D$.

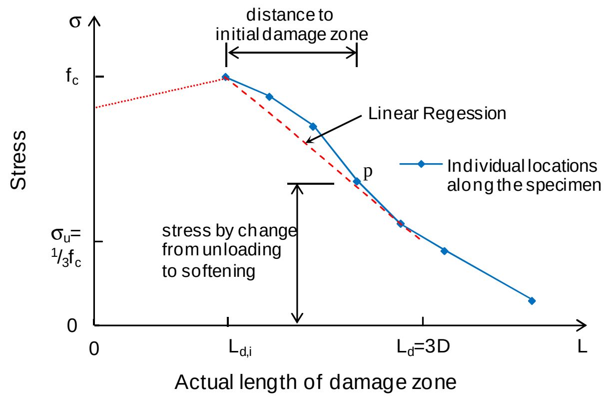

Figure 2: Extension of the damage zone (data adapted from Watanabe et al. 2004)

By reaching the peak stress, the length of the damage zone proposed by Lersrisakulrat et al. (2001) is adopted (Eq. (1)). This proposal considers influences of both specimen size and shape on the size of damage zone and can be also confirmed by other experimental test (Watanabe et al. 2004; Puri and Weiss 2006).

$$\begin{aligned} L_{d,i} &= 1.36\sqrt{A_c} && \text{with } \sqrt{A_c} < 100\,(mm) \\ &= 1.71 - 3.53 \cdot 10^{-5} \cdot A_c && \text{with } 100 \le \sqrt{A_c} \le 180\,(mm) \\ &= 0.57\sqrt{A_c} && \text{with } \sqrt{A_c} > 180\,(mm) \end{aligned} \tag{1}$$

In Fig. 2 shows the relation between the stress level, at which the strain behavior of a measured location in a specimen changes from unloading to softening, and the distance from this location to the *initial damage zone*, which is produced from the experimental results of Watanabe et al. (2004). At a stress of $\sigma_u = {}^{1}/_{3}\, f_c$ the damage zone propagates to a length of approx. $3\ D$, a linear regression for the growth of the damage zone is assumed.

With the proposed mechanism for the development of the damage zone during the failure, the actual length of the damage zone at a stress σ ($f_c \ge \sigma \ge {}^{1}/_{3}\, f_c$) is determined as:

$$L_{d,\sigma} = L_{d,i} + \frac{f_c - \sigma}{\frac{2}{3} f_c} \cdot \left(L_d - L_{d,i} \right) \tag{2}$$

Where $L_d = 3\,D$ is the ultimate length of the damage zone.

3. FRACTURE ENERGY IN COMPRESSION

The compressive fracture energy per unit specimen area corresponds to the area under the stress-displacement diagram. According to the proposal of Jansen and Shah (1997) two portions of the release energy are examined, i.e. the prepeak and postpeak energies as illustrated in Fig. 3.

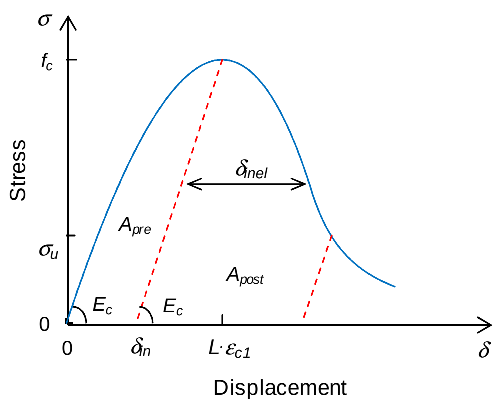

Figure 3: Fracture energy of concrete in compression (Jansen & Shah 1997)

The prepeak energy per unit specimen area (A_{pre}) corresponds to the dissipated energy by loading the specimen up to the peak stress and then unloading it completely. This portion is proportional to the compressive strength and the length of specimen and can be calculated by using a solidity factor of the ascending branch of the stress-strain curve of concrete.

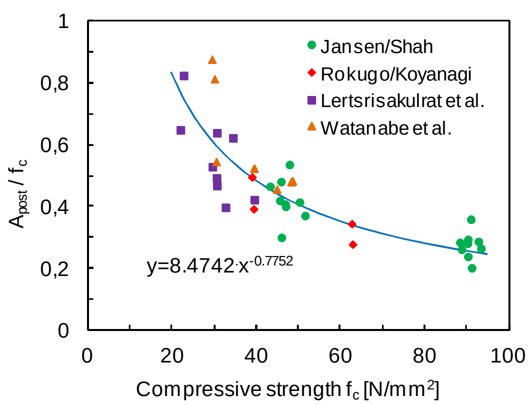

Figure 4: Compressive fracture energy versus compressive strength

The postpeak energy per unit specimen area is calculated from the area under the stress-inelastic displacement from the peak stress until $\sigma_u = {}^1\!/_3\, f_c$ in Fig. 3. This portion corresponds to the amount of energy dissipated for the crack formation and propagation during the failure. Thus only the experimental results obtained from specimens with the length-to-width $L/D \geq 3$ were used, in which the crack propagation can reach its maximum length. The selection of slender specimens reduces also the unfavorable influence of the boundary restraint, if exists.

From the experimental stress-displacement curves available in the literature (Rokugo and Koyanagi 1992; Jansen and Shah 1997; Lersrisakulrat et al. 2001; Watanabe et al. 2004) a proposal for the postpeak fracture energy is presented in Eq. (4). Fig 4 shows the results of the regression analysis.

$$A_{post} = 8.4742\, f_c^{0.2248} \tag{3}$$

As mentioned before Eq. (4) is valid only for specimens with $L/D \geq 3$. For shorter specimens with frictionless boundary condition the dissipated energy becomes smaller. This agrees well with the experimental results of (Vonk 1992; Lee and Willam 1997).

4. BEHAVIOR OF DIFFERENT ZONES IN A SPECIMEN

With the proposed mechanism of the localization the strain behavior in post-peak regime of a point in a specimen depends on its location and is determined by one of the following laws: elastic unloading; softening; or combination of unloading and softening.

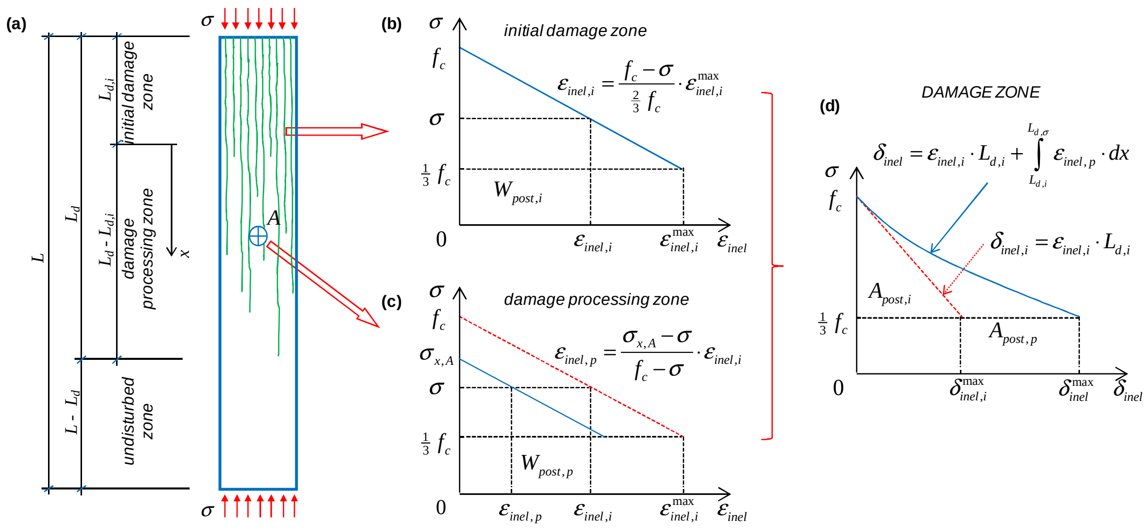

Figure 5: Postpeak inelastic strains of different zones in a specimen

Assumed that the softening law of all points in the damage zone is identical and can be described by a linear relation. The difference between particular points is determined by the beginning of the change from elastic unloading to softening. Therefore the strain of an arbitrary location in the *initial damage zone* at a stress σ is determined from the ultimate strain as (see Fig. 5(b)):

$$\varepsilon_{inel,i} = \frac{f_c - \sigma}{\frac{2}{3} f_c} \cdot \varepsilon_{inel,i}^{\max} \tag{4}$$

At an arbitrary location in the *damage processing zone* with a distance $L_{d,p}$ from the *initial damage zone* (point A in Fig. 5(a)) the strain behavior changes from the elastic unloading to softening at a certain level of stress $\sigma_{x,A}$. This stress can be calculated according to Eq. (2) as:

$$\sigma_{x,A} = f_c \cdot \left(1 - \frac{2}{3}\frac{L_{d,p} - L_{d,i}}{L_d - L_{d,i}}\right) \tag{5}$$

As the actual stress becomes lower than the stress $\sigma_{x,A}$ the post-peak inelastic strain in the *damage processing zone* can be calculated as (see Fig. 5(c)):

$$\varepsilon_{inel,p} = \frac{\sigma_{x,A} - \sigma}{f_c - \sigma} \cdot \varepsilon_{inel,i} \tag{6}$$

Inserting $\sigma_{x,A}$ from Eq. (5) in Eq. (6) it results then:

$$\varepsilon_{inel,p} = \left(1 - \frac{\frac{2}{3} f_c}{f_c - \sigma} \cdot \frac{L_{d,p} - L_{d,i}}{L_d - L_{d,i}}\right) \cdot \varepsilon_{inel,i} \tag{7}$$

The entire inelastic displacement of the specimen is then the integral of the postpeak inelastic displacements of all locations in the *initial damage zone* as well as the *damage processing zone* according to the illustration in Fig. 5(d) and can be written as:

$$\delta_{inel} = \varepsilon_{inel,i} \cdot L_{d,i} + \int_{L_{d,i}}^{L_{d,\sigma}} \varepsilon_{inel,p} \cdot dx \tag{8}$$

Substituting Eq. (4, 7) into Eq. (8), one can get:

$$\delta_{inel} = \frac{f_c - \sigma}{\frac{2}{3} f_c} \cdot \varepsilon_{inel,i}^{\max} \cdot L_{d,i} + \frac{1}{2}\left(\frac{f_c - \sigma}{\frac{2}{3} f_c}\right)^2 \cdot \varepsilon_{inel,i}^{\max} \cdot \left(L_d - L_{d,i}\right) \tag{9}$$

The inelastic displacement is a second order parabolic to the stress and reaches its maximum value at the ultimate stress $\sigma_u = {}^{1}/_{3}\, f_c$. From Eq. (9) it can be drawn:

$$\delta_{inel}^{\max} = \frac{2}{3}\left(L_d + L_{d,i}\right) \cdot \varepsilon_{inel,i}^{\max} \tag{10}$$

The post-peak energy per unit specimen area shown as A_{post} in Fig. 3 corresponds to the area under the curve defined by the σ-δ_{inel} displacement of Fig. 5(d).

$$A_{post} = \int_{f_c}^{f_c/3} \delta_{inel} \cdot d\sigma + \frac{f_c}{3} \cdot \delta_{inel}^{\max} \tag{11}$$

Inserting Eq. (9, 10) in Eq. (11) and solving the Eq. (11) according to $\varepsilon_{inel,i}^{\max}$ one gets:

$$\varepsilon_{inel,i}^{\max} = \frac{A_{post}}{\left(\frac{5}{18} L_d + \frac{7}{18} L_{d,i}\right) \cdot f_c} \tag{12}$$

It can be seen that the ultimate postpeak inelastic strain depends not only on the compressive strength but also on the length of damage zone. In other words the postpeak strain behavior is not pure material property, but a specimen character. Once the size and shape of a specimen are known the descending branch of the stress-displacement curve can be determined with Eq. (9).

5. COMPLETE STRESS-STRAIN CURVE

As the ascending branch of the stress-strain curve of concrete in compression is not affected from the specimen geometry and boundary condition, the relation between σ_c and ε_c of Model Code 2010 (2012) described by Eq. (13) is adopted. For the sake of simplicity other related material properties (E_{ci}, ε_{c1}) of this Code that are directly related to the compressive strength are also adopted.

$$\sigma_c = \left(\frac{k \cdot \eta - \eta^2}{1 + (k-2) \cdot \eta} \right) \cdot f_{cm} \tag{13}$$

Considering the specimen geometry the behavior after peak stress can be described by an average stress-strain relation:

$$\sigma_c = f_{cm} - \left(\varepsilon_c - \varepsilon_{c1} - \frac{\delta_{inel}}{L} \right) \cdot E_{ci} \tag{14}$$

6. COMPARISON WITH EXPERIMENTAL TESTS

Thirty specimens of two different compressive strengths, nominally 45 and 90 MPa, were tested to investigate the effect of length on the strain-softening of concrete (Jansen and Shah 1997). Two specimens for each of the length-to-width ratios (*L/D*) of 2.0, 2.5, 3.0, 3.5, 4.5 and 5.5 plus one of *L/D* of 4.0 were cut from the cylinder with diameter of 100 mm for each batch of concrete. Fig. 6 shows the experimental and the analytical stress-strain curves of six specimens with the *L/D* from 3.5 to 5.5. The difference of the strain at peak stress between analytical curves and tests increases slightly with the specimen length. Though, the agreement between the experimental and the analytical curves is satisfactory for both the ascending and the descending branches.

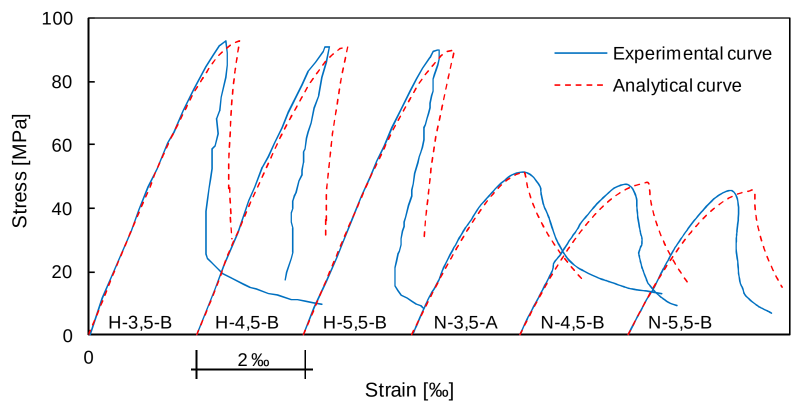

Figure 6: Total stress versus strain curves for some specimens of Jansen and Shah (1997)

7. CONCLUSION

Based on the observation of the crack propagation during the failure by tests without boundary restraint a new mechanism of the localization is presented. With the proposed mechanism the strain-softening behavior of different regions in the damage zone is separately determined.

It is shown through compression test on specimens of different lengths that the proposed model is realistic. Concerning the localization of failure in reinforced concrete members that the confinement effect is only activated in the damage zone with high deformation capacity, the determination of the stress-strain relation for *the initial damage zone* is of importance.

REFERENCES

Bazant, Z. P. (1989). Identification of strain-softening constitutive relation from uniaxial test by series coupling model for localization. *Cement and Concrete Research, 19*, pp. 973-977.

Dhir, R. K., & Sangha, C. M. (1974). Development and propagation of microcracks in plain concrete. *RILEM Materials and Structures, 7*, pp. 17-23.

International Federation for Structural Concrete. (2012). *Model Code 2010, Final draft* (Vol. 2). Lausanne: International Federation for Structural Concrete.

Jansen, M., & Shah, S. (1997). Effect of length on strain compressive strain softening of concrete. *J. Eng. Mech., ASCE, 123*(1), pp. 25-35.

Lee, Y., & Willam, K. (1997). Mechanical properties of concrete in uniaxial compression. *ACI Mater. J., 94*(6), pp. 457-471.

Lersrisakulrat, T., Watanabe, K., Matsuo, M., & Niwa, J. (2001, Dec.). Experimental study of localization parameters in concrete subjected to compression. *Concrete Library of JSCE, 38*, pp. 225-236.

Markeset, G. (1993). Failure of concrete under compressive strain gradients. *Ph.D. thesis*. NTH University of Trondheim.

Puri, S., & Weiss, J. (2006). Assessment of localized damage in concrete under compression using acoustic emission. *J. Mater. Civ. Eng., ASCE, 18*(3), pp. 325-333.

Rokugo, K., & Koyanagi, W. (1992). Role of compressive fracture energy of concrete on the failure behavior of reinforced concrete beams. In A. Carpinteri, *Applications of fracture mechanics to reinforced concrete* (pp. 437-464). Elsevier Applied Science.

Shah, S. P., & Sankar, R. (1987). Internal cracking and strain-softening response of concrete under uniaxial compression. *ACI Mater. J., 84*, pp. 200-212.

Torrenti, J. M., Desrues, J., Benaija, E. H., & Boulay, C. (1991). Stereophotogrammetry and localization in concrete under compression. *J. Eng. Mech., ASCE, 117*(7), pp. 1455-1465.

van Mier, J. G. (1984). Strain-softening of concrete under multiaxial loading conditions. *Ph.D. thesis*. Technische Hogeschool Eindhoven.

Van Mier, J. G. (2009). Mode II fracture localization in concrete loaded in compression. *J. Eng. Mech., ASCE, 135*(1), pp. 1-8.

Vonk, R. A. (1992). Softening of concrete loaded in compression. *Ph.D. thesis*. University of Eindhoven.

Watanabe, K., Niwa, J., Yokota, H., & Iwanami, M. (2004). Experimental study on stress-strain curves of concrete considering localised failure in compression. *Journal of Advanced Concrete Technology*(2), pp. 395-407.